Viscoelastic and Shrinkage Behavior of Ultrathin Polymeric Films

BRIAN L. WEICK and BHARAT BHUSHAN*

Computer Microtribology and Contamination Laboratory, 206 W. 18th Avenue, The Ohio State University, Columbus, Ohio 43210-1107

SYNOPSIS

Viscoelastic and shrinkage characteristics of five ultrathin polymeric films are presented. These films include poly(ethylene terephthalate) or PET, poly(ethylene naphthalate) or PEN, an aromatic polyamide (ARAMID), a polyimide (PI), and poly(benzoxazole) or PBO. PET film is currently the standard substrate used for magnetic tapes, and the other four films represent alternative substrates with improved material properties. Thicknesses of the films range from 14.4 μm for PET to 4.4 μm for ARAMID. A creep apparatus is used to measure the viscoelastic and shrinkage characteristics of the films. The largest amount of creep compliance was measured for PET followed by PI, PEN, ARAMID, and PBO. Creep velocity was highest for PET and PI, followed by ARAMID, PEN, and PI. Shrinkage measurements at 50°C for 100 h show that PEN shrinks more than all the other substrates. Time–temperature superposition is used to predict long-term creep behavior, and relationships between polymeric structure and viscoelastic behavior are also discussed. Based on their relative cost and creep behavior, PEN and ARAMID substrates appear to be suitable alternatives to PET. © 1995 John Wiley & Sons, Inc.

INTRODUCTION

Poly(ethylene terephthalate), or PET, is currently the most widely used polymeric substrate material for magnetic recording tapes.[1] Thinner substrates and high areal densities (track density × linear density) are required to increase volumetric density. For high areal densities, a substrate with high mechanical and environmental stability and high surface smoothness is required. For high track densities (i.e., low track pitch), lateral contraction of the substrate due to thermal, hygroscopic, viscoelastic, and/or shrinkage effects must be minimal during storage on a reel and use in a drive. In linear tape drives, linear deformations can be accommodated by a change in clocking speed. However, in rotary tape drives, anisotropic deformation of the substrate is undesirable. To minimize stretching during use of thinner substrates, the modulus of elasticity, yield strength, and tensile strength should be high along the machine direction. Furthermore, because high coercivity magnetic films on metal evaporated tapes are deposited and/or heat treated at elevated temperatures, a substrate with stable mechanical properties up to a temperature of 100–150°C or even higher is desirable. Because magnetic recording devices require low motor torque and high magnetic reliability, the finished magnetic medium must also exhibit low friction/stiction and high durability. For an advanced tape storage device with a volumetric density of one terabyte per cubic inch, the following characteristics are required: a tape substrate that is approximately 4 μm thick, a magnetic medium with a track density of about 9000 tracks per inch, and a linear density of about 160 kbits/inch with a 64 head array and eight head positions. Because of limitations in fabrication of narrow track heads, data can be read from only 256 tracks while scanning in a data recovery mode. Therefore, for a 12.7 mm wide tape, if a 10% track mismatch is tolerable, shrinkage of less than about 5.0 μm in the transverse direction is desirable, provided that the head can be recentered. As the tape is unwound and goes over the head, elastic/viscoelastic recovery in the first few

* To whom correspondence should be addressed.

Journal of Applied Polymer Science, Vol. 58, 2381–2398 (1995)
 CCC 0021-8995/95/132381-18

milliseconds is important and requires optimization of transient properties. In addition to mechanical and environmental stability, the cost of the material is also a major factor in the selection of a suitable substitute for PET.[1]

Viscoelasticity refers to the combined elastic and viscous deformation of a substrate when external forces are applied, and shrinkage occurs when residual stresses present in the substrate are relieved at elevated temperatures.[1-5] Because shrinkage is a nonrecoverable deformation process, if the substrate of a magnetic storage tape shrinks, the head will not be able to read back information on that tape. Similarly, if a substrate deforms viscoelastically, information stored on the tape could also be lost. Various long-term reliability problems including uneven tape-stack profiles (or hardbands), mechanical print-through, instantaneous speed variations, and tape stagger problems can all be related to the substrate's viscoelastic characteristics.[1] To minimize these reliability problems, it is not only important to minimize creep strain, but the rate of increase of total strain needs to be kept to a minimum to prevent stress relaxation in a wound reel.

Alternative substrates being considered include poly(ethylene naphthalate) or PEN, a polyimide (PI), an aromatic polyamide (ARAMID), and poly(benzoxazole) or PBO. Perettie et al.[6,7] have presented some material property information about these advanced substrates including shrinkage characteristics at 200°C. Perettie and Speliotis[8] have recently addressed issues pertaining to the effect of substrate materials and environment on the stability of advanced magnetic media, and they also addressed the need for substrate materials with improved mechanical, thermal, and hygroscopic characteristics. Although extensive research has been performed on PET to determine its viscoelastic and shrinkage characteristics,[1] information pertaining to such characteristics of the alternative polymeric films is not readily available.

The main objective of this research was to measure viscoelastic characteristics of polymeric films that are typically used as substrates for magnetic tapes. The specific viscoelastic property measured was creep compliance. Experiments were carried out at temperatures ranging from ambient to 50°C, which is the upper design limit for magnetic tapes. From these measurements the rate of creep was predicted, and lateral contraction of the substrate due to Poisson effects was determined. Time–temperature superposition was used to predict long-term viscoelastic behavior. It was also desirable to evaluate creep recovery characteristics. Shrinkage measurements were made to determine the extent of nonrecoverable deformation undergone by the materials at elevated temperatures, and both viscoelastic and shrinkage behavior were related to the structural characteristics of each polymer.

EXPERIMENTAL TECHNIQUE

Test Apparatus

Viscoelastic and shrinkage characteristics of the polymeric materials were evaluated using the apparatus shown in Figure 1. Up to five tape specimens were tested simultaneously using this apparatus, and viscoelastic properties at elevated temperature and/or humidity levels could be obtained by performing experiments in an environmental chamber. The apparatus consisted of five balance beams (or load arms), and polymeric films were fixed at the end of each balance beam and aligned with a straight edge. A linear variable differential transformer (LVDT) was connected to the other end to measure deflection of the load arm due to creep of the tape substrate, and the LVDT output was recorded on a PC. Because the apparatus was placed in an environmental

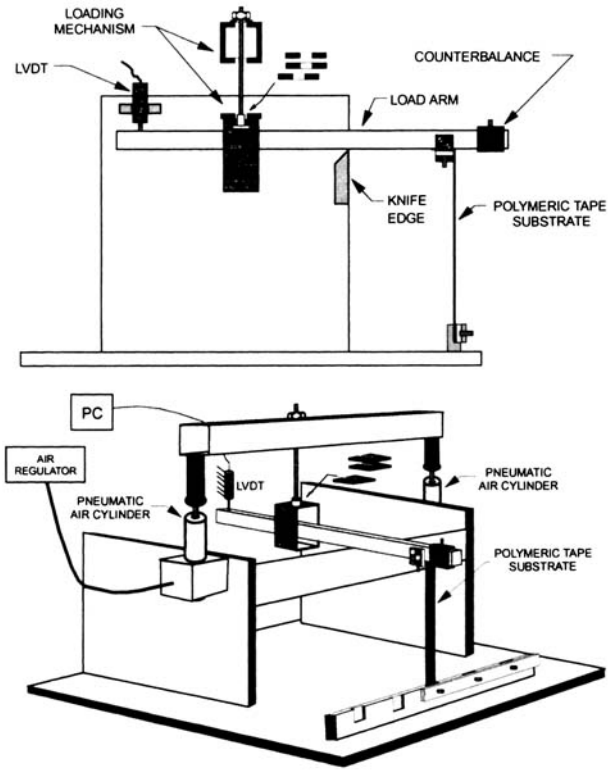

Figure 1 Experimental apparatus for evaluating the creep and shrinkage behavior of ultrathin polymeric films.

Table I List of Ultrathin Polymeric Films

	Material	Manuf. Method	Trade Name	Supplier	Thickness (μm)
PET	Poly(ethylene terephthalate)	Drawing	Mylar A (57DB)	Dupont	14.4
PEN	Poly(ethylene naphthalate)	Drawing	Teonex	Teijin	4.5
ARAMID	Aromatic poly(amide)	Casting	Mictron TX-1	Toray	4.4
PI	Poly(imide)	Casting	Upilex	Ube	7.6
PBO	Poly(benzoxazole)	Casting	—	Dow	5.0

chamber, the balance beams were loaded remotely using a pneumatically controlled mechanism. As shown in Figure 1, weights were placed on top of rectangular pieces positioned around each load arm. These rectangular pieces were suspended from a single crossmember (a square tube), and lowering or raising this crossmember using air cylinders controlled the loads imposed on the balance beams.

Test Specimens

Table I provides a list of the polymeric films examined in this research. The suppliers of the films are also listed along with the trade name where applicable. The 14.4 μm thick PET film examined in this study is the typical database grade material used as substrates for magnetic tapes. Tensilized PEN is beginning to see some use as a substrate for long-play video tapes and high capacity QIC data cartridges, and the Sony NTC-90 Digital Micro Tapes used in the Scoopman™ Digital Microrecorders consist of a metal-evaporated coating on an ARAMID substrate. Both PEN and ARAMID are currently available in thicknesses as low as 4.4 μm, but ARAMID is manufactured using a relatively expensive solution casting process, whereas PEN is manufactured by a drawing process in the same manner as PET. The PI and PBO polymers included in this study are developmental materials with characteristics that could be suitable for magnetic tapes.[1,6-8] They are also manufactured using a solution casting process, and are available in thicknesses of 7.6 μm for PI and 5.0 μm for PBO. The solution casting process virtually eliminates the shrinkage, which is common in drawing processes. However, the cost of the film produced by casting is much higher and, therefore, PBO is believed to be the most expensive to manufacture.

The chemical structures of the respective polymeric materials are shown in Figure 2. PET and PEN have identical hydrocarbon backbones indicative of polyester materials. However, PET contains a single benzene ring in each repeat unit, whereas PEN contains a naphthalene ring. ARAMID and PBO are often referred to as liquid crystal polymers because they form oriented liquid crystalline arrays in solution.[6,9] As a result, the polymers have rigid rod-like structures that exhibit a high degree of orientation, and enable the formation of high-strength, high-modulus films. As shown in Figure 2, polyimides are also high-strength, high-modulus films due to their rigid, aromatic, macromolecular structure.[10]

Experimental Procedure

For both creep and shrinkage experiments the samples were cut with a scalpel blade into 190 mm long

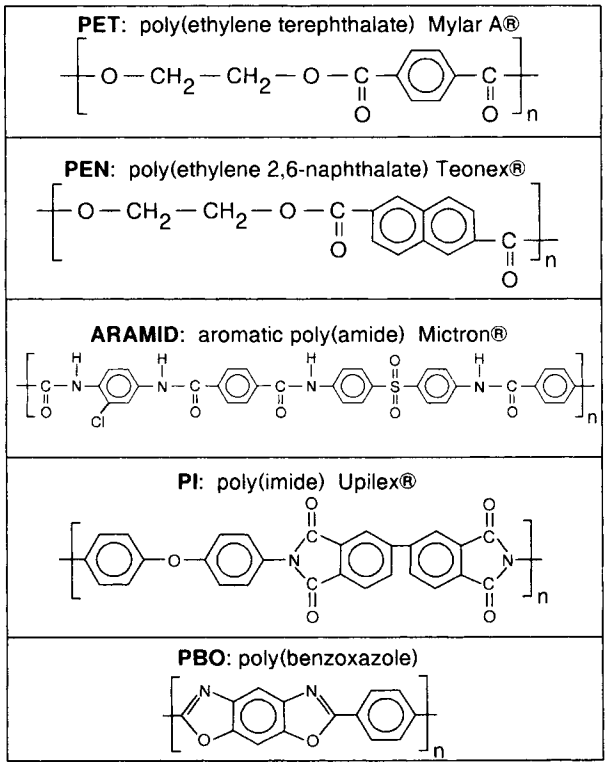

Figure 2 Chemical structures of ultrathin polymeric films.

by 12.7 mm wide strips to accommodate the creep tester and size of the environmental chamber. Prior to loading the samples, the environmental chamber was turned on to stabilize the temperature in the chamber and allow the structure of the creep tester to undergo any dimensional changes. During this stabilization period of typically 1 to 2 h the signals from the LVDT's were monitored until they were steady. At this point the chamber was opened and the samples were fastened between the load arms and base of the creep tester. A preload of 0.5 MPa was applied to the specimens by adjusting the counterbalance weight on the load arm. The chamber was then closed and allowed to return to its preset temperature before beginning an experiment. A description of specific procedures for the creep and shrinkage experiments follows, and the test conditions are summarized in Table II.

For the creep experiments, the samples were loaded to 7.0 MPa using the pneumatic control mechanism. This relatively low stress has been shown to keep the creep experiments in the linear viscoelastic regime.[1] Preliminary experiments at higher stresses using the films studied herein also showed that nonlinear viscoelastic behavior did not occur. For the first hour, the sampling rate for the data acquisition system was set to 12.5 samples/sec per load arm, and 25 data points acquired into memory were averaged for each data point written to the computer's hard disk. After 1 h the sampling rate was slowed down to 0.25 samples/sec with the same averaging scheme. Creep characteristics of the specimens were monitored for an additional 99 h. At the end of the 100 h experiment the sampling rate was once again increased to 12.5 samples/sec per load arm, and the specimens were pneumatically unloaded. Recovery characteristics were then monitored at the lower sampling rate for approximately 10 h or until the signals reached a steady level.

Shrinkage experiments were performed at 50°C using the 0.5 MPa load initially applied to the specimens after they were fastened to the grips. This minimal load was required to hold the films between the grips without causing any substantial creep of the specimens. Shrinkage experiments were performed for 100 h. A sampling rate of 0.25 samples/sec per load arm was used, and 25 samples acquired into memory were averaged for each data point written to the hard disk.

Table II Test Conditions

Creep Experiments	
Temperatures: 25, 40, and 50°C	
Duration of experiments: 100 h	
Applied stress:	7.0 MPa (PET, PEN, ARAMID, PI)
	14.0 MPa (PBO)
Relative humidity: 15–25%	
Shrinkage Experiments	
Temperature: 50°C	
Duration of experiments: 100 h	
Applied stress: 0.5 MPa	
Relative humidity: 15–25%	

DATA REDUCTION METHODS

During an experiment the LVDTs connected to each load arm measure the change in length of each polymeric film. This change in length is, in general, a nonlinear function of time (and temperature) for polymers. The amount of strain the film is subjected to can be calculated by normalizing the change in length of the specimen with respect to the original length. Creep compliance can then be calculated by dividing the time-dependent strain by the constant applied stress:

$$\varepsilon(t) = \frac{\Delta l(t)}{l_o} \tag{1}$$

$$D(t) = \frac{\varepsilon(t)}{\sigma_o} = \frac{\Delta l(t)}{\sigma_o l_o} \tag{2}$$

where,

$\Delta l(t)$ ≡ change in length of the polymeric film as a function of time.
l_o ≡ original length of the polymeric film.
$\varepsilon(t)$ ≡ the amount of strain the film is subjected to.
σ_o ≡ constant applied stress.
$D(t)$ ≡ tensile creep compliance of the polymeric film as a function of time.

Creep compliance data for the polymeric films are modeled using a generalized Kelvin–Voigt model that has the following mathematical form:

$$D(t) = D_o + \sum_{k=1}^{K} D_k[1 - \exp(-t/\tau_k)] \tag{3}$$

where,

D_o ≡ instantaneous compliance at time $t = 0$.
D_k ≡ discrete compliance terms for each Kelvin–Voigt element.
τ_k ≡ discrete retardation times for each Kelvin–Voigt element.

Based on this model, for a constant stress of magnitude σ_o applied at $t = 0$, the instantaneous

response of a viscoelastic solid will be a sudden strain of magnitude $\varepsilon_o = \sigma_o D_o$. This is followed by a delayed (or retarded) response that can be attributed to the additional exponential terms in eq. (3). More specifically, each kth element of the model contributes a delayed compliance of magnitude $D_k[1 - \exp(-t/\tau_k)]$, and the amount of this delay is directly related to the magnitude of the retardation times τ_k.[2,3]

Equation 3 is typically represented as a series of parallel springs and dashpots connected to a single spring. This mechanical analog is shown in Fig. 3, and is indicative of a viscoelastic polymer which has an amorphous phase with mainly unoriented molecules, and a crystalline phase which contains oriented molecules. Components of the polymeric structure which respond instantly to an applied stress are modelled as a single spring with an instantaneous compliance D_o. Components of the polymeric structure which do not respond instantly but are deformed in a time-dependent manner are modelled as multiple elements consisting of springs and dashpots acting in parallel. Each element contains a spring which has a compliance D_k, and a dashpot with a viscosity equal to η_k. The retardation time for each kth element is defined below:

$$\tau_k = \eta_k D_k \tag{4}$$

Note that the retardation time can also be interpreted as the length of time required to attain $(1 - 1/e)$ or 63.2% of the equilibrium strain for each element.[1-4]

Experimental data sets are fitted to Eq. (3) using a nonlinear least-squares technique known as the Levenberg–Marquardt method.[11] This method is used to find the best-fit parameters τ_k and D_k for a Kelvin–Voigt model with multiple elements. Typically, two to three elements are required for a reasonable fit.

RESULTS AND DISCUSSION

Creep Compliance Measurements and Analysis

Because the motivation for this study was to characterize alternative substrates for magnetic tapes, experiments were performed at a 50°C temperature level, which is the typical upper storage limit for magnetic tapes.[1] For this reason, experimental results presented in this section will be for a 50°C temperature level, and differences between the polymeric films will be emphasized. (See the section on time–temperature superposition for a discussion of results at other temperatures.) Curve fits using the data reduction techniques discussed above will first be presented followed by a more detailed discussion of the creep measurements and characteristics. Lateral strain calculations based on Poisson effects will also be discussed, and creep velocity characteristics obtained by differentiating the creep data will also be summarized.

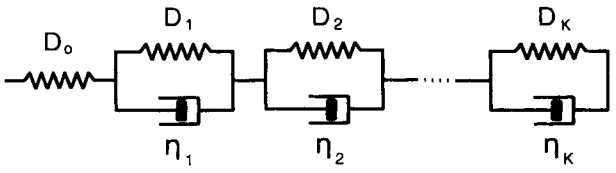

Figure 3 Generalized Kelvin–Voigt model.

Experimental Data and Curve Fits

Figure 4 shows creep compliance measurements and curve fits at 50°C for the ultrathin polymeric substrates. Curve fits using a two-term Kelvin–Voigt model are shown as dashed lines, and curve fits using a three-term model are shown as solid lines. Experimental data points are represented as open circles, and not all of the 100 data points used in the curve fitting procedure are shown. This is due to the fact that the graphs in Figure 4 are presented on a log–log scale to accentuate any lack of fit at the shorter time periods (i.e., less than 1 h). When the data is represented on a linear scale, no lack of fit is observed at the longer time periods. Note that the D_o term in Eq. (3) is not included in the curve-fitting procedure. For all the experiments it is taken as the initial data point acquired at approximately time = 0. Therefore, in Figure 4 this D_o term is subtracted out to show how well the model fits the data. In later figures, this term is simply readded to the data sets.

Data sets and curve fits are only shown in Figure 4 for the machine direction (major optical axis for PET), and data sets for the transverse direction (minor optical axis for PET) are fitted in the same manner. From a visual inspection, it is clear that a three-term model fits the data better than a two-term model. For all the materials but PBO, the two-term models do not fit the data at time periods less than 1 h, and the three-term models provide a much better fit. For PBO, there is some lack of fit at time periods less than 0.1 h for both two- and three-term models. However, both curve fits are adequate at longer time periods.

Because three individual elements are used to fit each data set, three retardation times and three compliance terms can be tabulated for each material. These values are shown in Table III along with the instantaneous compliance, D_o. For each element, at

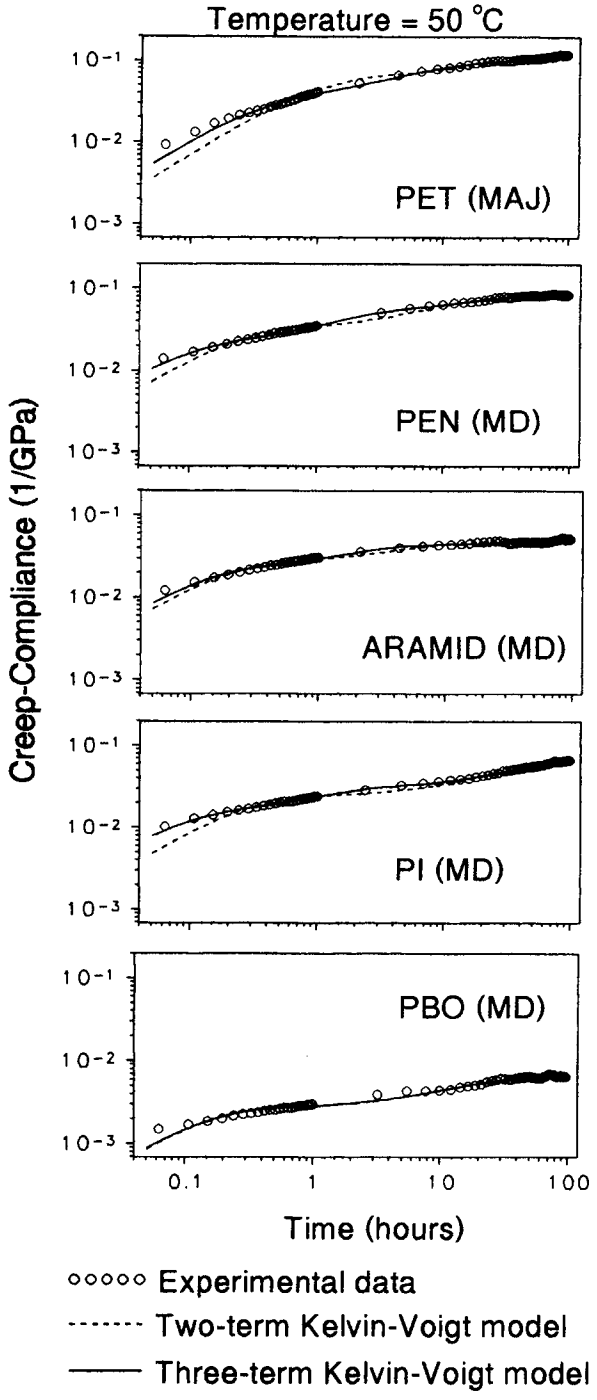

Figure 4 Experimental creep data and curve fits for ultrathin polymeric films plotted on a log–log scale. The initial compliance term (D_o) has been subtracted out.

higher retardation times the value of the exponential term $1/\exp(t/\tau_k)$ increases. As a result, because the delayed compliance for each element is $D_k[1 - 1/\exp(t/\tau_k)]$, higher retardation times correspond with lower creep compliance contributions from each element. However, one should be cautioned not to draw conclusions from a comparison of tabulated retardation times for individual elements, especially when more than just one or two are utilized. As shown by Eq. (5), the total compliance is due to the addition of compliance contributions from each element, and for comparative purposes the data must be plotted as shown in Figures 4 and 5.

In the limit as the retardation times go to infinity for an element, the compliance contribution for that element becomes negligible. This is the case for ARAMID, PI (TD), and PBO. The third elements for these materials have retardation times that are five to seven orders of magnitude different from the other retardation times. Regardless of whether or not these retardation times are positive or negative large numbers, the exponential term $1/\exp(t/\tau_k)$ will be nearly 1.0 and the delayed compliance for this element will be zero. Note that these large retardation times are still determined as part of the three-term curve fit for ARAMID, PI (TD), and PBO. Furthermore, they seem to ensure that the other two elements have optimal compliance and retardation values.

Creep Compliance Measurements

Creep compliance measurements for PET and the alternative substrate materials are shown in Figure 5(a) and (b) for a 50°C temperature level. The data sets are plotted on a linear scale in Figure 5(a), and on a log–log scale in Figure 5(b). Curve fits using the Marquardt algorithm are shown in these figures, and two material orientations are shown for each of the five polymer films. In addition, the initial data point has been readded to the data sets. Recall that this data point was subtracted off for the curve-fitting procedure. Although this initial point is modeled as the instantaneous compliance D_o, it is indicative of both elastic and short-term viscoelastic responses. These short-term responses occur at a rate that is faster than the 0.5 Hz sampling rate used during the first hour of the experiments. Throughout the rest of the 100-h experiments the materials creep (or stretch) due to the viscoelastic characteristics of the particular polymeric material being evaluated.

Overall, from Figure 5(a) and (b), the total amount of creep compliance for PET is typically higher than that measured for the alternative substrates. PEN oriented in the transverse direction, PEN (TD), creeps slightly more than PET does along its major optical axis. However, the creep compliance for PEN (MD) is significantly less than that measured for PET along both major and minor optical axes. The polyimide material (PI) also shows

Table III Discrete Compliance Terms (D_k) and Retardation Times (τ_k) for Ultrathin Polymeric Films

		D_0 1/GPa	D_1 1/GPa	τ_1 h	D_2 1/GPa	τ_2 h	D_3 1/GPa	τ_3 h
PET	MAJ	0.228	0.031	0.287	0.059	5.84	0.116	320.0
	MIN	0.309	0.031	0.189	0.079	5.19	0.082	91.7
PEN	MD	0.146	0.019	0.073	0.03	1.49	0.037	18.4
	TD	0.221	0.032	0.059	0.048	1.28	0.058	20.7
ARAMID	MD	0.121	0.021	0.103	0.023	2.09	4.5 E2	5.5 E6[a]
	TD	0.095	0.020	0.285	0.027	4.45	−2.2 E3	1.2 E7[a]
PI	MD	0.255	0.014	0.068	0.016	1.04	0.046	54.1
	TD	0.189	0.021	0.172	0.025	12.5	−1.4 E2	−4.2 E5[a]
PBO	MD	0.062	0.003	0.124	0.004	15.0	21.06	6.0 E6[a]
	TD	0.060	0.002	0.104	0.002	6.57	−7.37	−1.0 E6[a]

Temperature = 50°C.
[a] The magnitude of these terms indicates that the contribution from this Kelvin–Voigt element is negligible.

an improvement in total creep compliance when compared to PET. However, this improvement is only slight for PI (MD), and the total creep compliance for PEN (MD) is lower than that measured for PI in either orientation. Creep compliance measurements for ARAMID and PBO tend to fall well below the measurements for PET, PEN, and PI. The total compliance for PBO (MD and TD) is relatively constant at 0.65 GPa^{-1}. ARAMID does not show quite as much improvement in creep compliance as PBO, but the total amount of compliance (ranging from 0.16 to 0.18 GPa^{-1}) is still less than that measured for PET, PEN, or PI.

Throughout the 100 h experiments, the total creep compliance measurements for PET (MIN) are typically 0.12 GPa^{-1} higher than the compliance for PET (MAJ). A similar amount of anisotropy is observed for PEN. Creep compliance measurements for PEN (TD) are also typically higher than those for PEN (MD), with a difference of 0.10 GPa^{-1}. In comparison, unlike the PET or PEN materials, PI, ARAMID, and PBO have creep compliances that are actually higher in the machine direction than the transverse direction. Furthermore, these materials tend to be more isotropic. The creep compliance for PI (MD) is approximately 0.5 GPa^{-1} higher than the compliance for PI (TD), and the difference between compliances for ARAMID (MD) and ARAMID (TD) is less than 0.1 GPa^{-1} at the end of the 100 h experiments. PBO shows an immeasurable amount of anisotropy in its creep compliance behavior.

Lateral Strain Calculations

To further quantify the viscoelastic behavior of polymer films, the amount of lateral strain due to Poisson effects can be calculated. Because magnetic tapes are placed under tension in a tape drive, any lateral strain associated with the applied tension will cause the tape to contract. This can lead to "read errors" if there is a mismatch between tracks on the tape and tracks on the head. Therefore, a minimal amount of lateral strain is desirable if the polymeric film is used as a substrate for magnetic tapes.[1,12] Calculated lateral strains are shown on the right-hand axis of Figure 5(b). These contractions were calculated using a Poisson's ratio of 0.3, which has been shown to be a valid number for PET.[1] This is also a valid approximation for the other polymeric films.[9] The largest amount of lateral strain was measured for PET (approx. 0.094% along the minor axis), and the least amount of strain was measured for PBO (0.025–0.026%). PEN and PI show 0.048 to almost 0.070% lateral strain depending on the material orientation, whereas ARAMID shows only 0.035–0.038% lateral strain.

Creep Velocity Calculations

From the slopes of the creep compliance curves in Figures 5(a) and (b), the rate of creep can be determined. Because the data sets have been fitted to the Kelvin–Voigt model, the first derivatives of the creep compliance curves can be explicitly calculated using the first derivative of Eq. (3).

$$\frac{dD(t)}{dt} = \sum_{k=1}^{K} \frac{D_k}{\tau_k} \exp(-t/\tau_k) \qquad (5)$$

where, $dD(t)/dt \equiv$ rate of creep compliance or "creep velocity" in $1/(GPa \cdot h)$.

Creep velocity calculations are shown in Figure 6 on a log–log scale. PBO appears to creep at the lowest

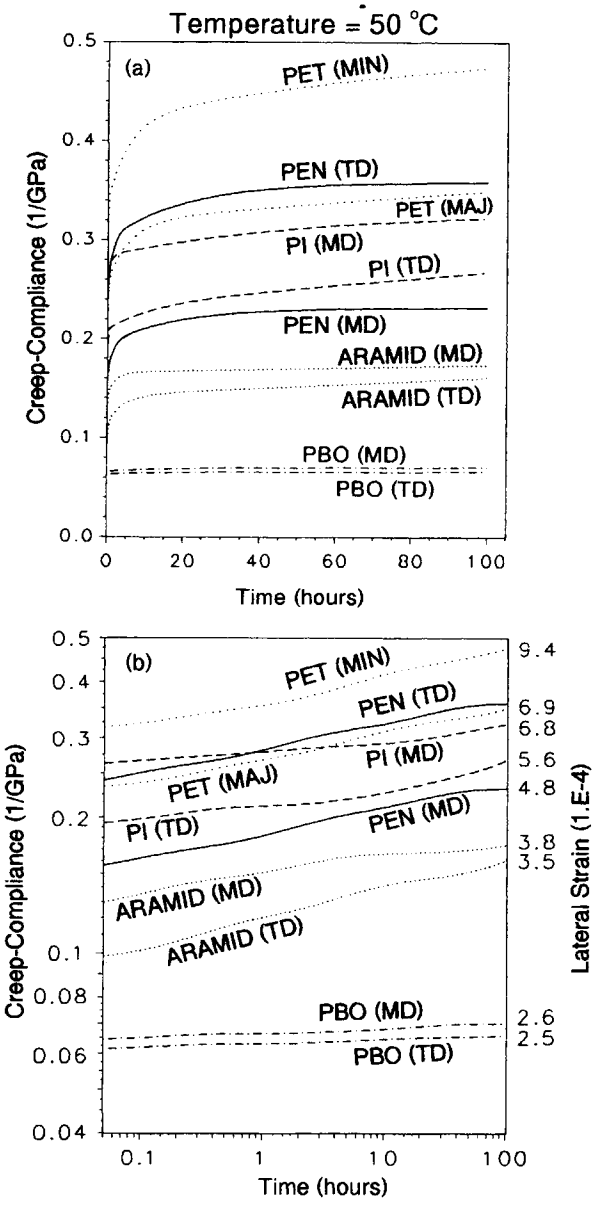

Figure 5 Creep compliance measurements for ultrathin polymeric films plotted on (a) linear axes, and (b) log–log axes. The right-hand axis in Figure 5(b) shows lateral strain calculations assuming a Poisson's ratio of 0.3.

rate throughout the 100 h experiments. When compared to PET, PI offers only a slight improvement in creep velocity; whereas the creep velocity for ARAMID is always lower than the velocity for PET. During the first part of the experiment PEN creeps at a rate that is nearly equal to the creep velocity for PET. However, at the end of the experiment, the creep velocity for PEN is an order of magnitude lower than the velocity for PET. PEN also creeps at a lower rate than ARAMID after 100 h.

Figure 6 not only shows relative creep rates for the materials, additional information can be extracted from the slopes of the creep velocity curves. These slopes indicate acceleration (or deceleration) during the creep process. Typically, the materials show a decreasing creep velocity and a negative slope, which indicates deceleration during the creep process. For ARAMID, the slope of the creep velocity curve remains constant after 100 h. This means that ARAMID continues to creep at the same rate without a change in velocity. In comparison, PEN not only creeps at a lower rate than ARAMID after 100 h, but the changing slope of the curves for PEN indicates that the creep velocity for PEN is decreasing. Recall from Figures 5(a) and (b) that the total creep for ARAMID is actually less than the total creep for PEN. However, from this discussion, PEN actually creeps at a lower rate than ARAMID, and this rate shows a decreasing trend after 100 h.

Creep Recovery Characteristics

At the end of a creep compliance experiment the loads imposed on the samples are lifted off using the pneumatic control mechanism. As a result, each polymeric material undergoes a recovery process. Ideally, a polymer should recover its initial elastic deformation immediately. However, the viscoelastic deformation is not recovered immediately, and is a time-dependent phenomenon that occurs at a rate

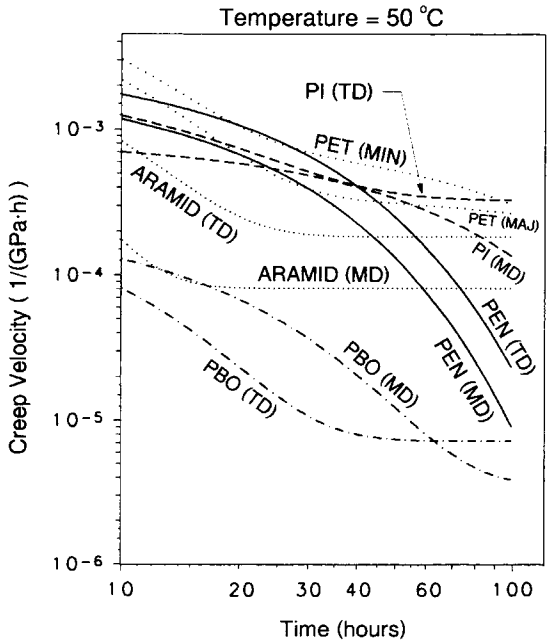

Figure 6 Creep velocity measurements for ultrathin polymeric films.

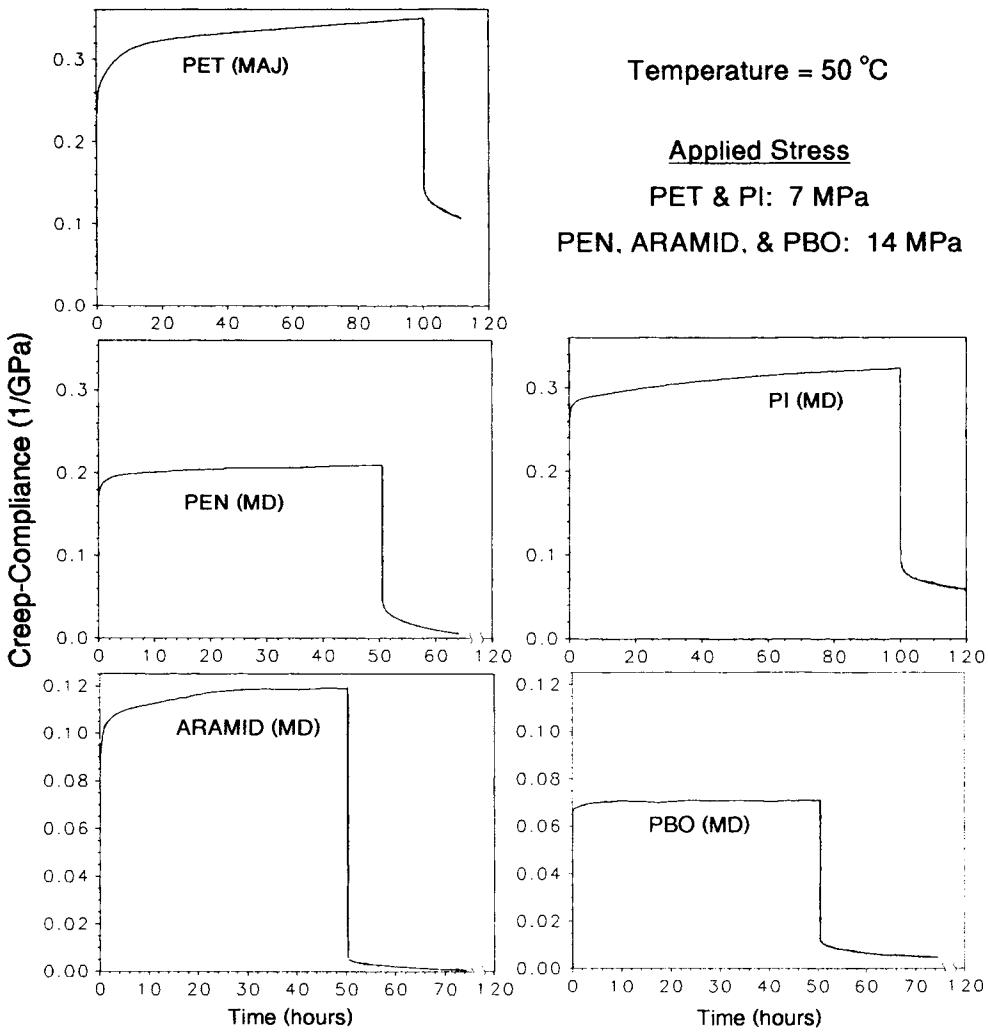

Figure 7 Typical creep recovery characteristics for ultrathin polymeric films.

that is equal to the original rate of creep. Figure 7 demonstrates this for PET, PEN, ARAMID, PI, and PBO. Typical creep compliance data sets are shown in this figure for the machine direction or major optical axis (PET). Data sampled after the creep experiments show the recovery characteristics for each material.

Creep compliance and recovery characteristics for PET are shown at the top of Figure 7. At time zero the load is applied causing an immediate elastic response followed by a viscoelastic response. At the 100 h point the load is removed and the polymeric film begins to recover. Due to removal of the load there is a rapid decrease in compliance that occurs almost immediately. This rapid decrease is indicative of the elastic and short-term (immeasurable) viscoelastic behavior of the material. The long-term viscoelastic behavior is measured for the next 20 h, and occurs at a rate that should be equal (but opposite) to the rate of creep. However, unlike PEN, ARAMID, and PBO the creep–recovery curve for PET does not tend to zero after 10 to 20 h of recovery. Instead, the recovery curve for PET tends to level off at a value somewhat less than 0.1 GPa^{-1}. This behavior for PET has also been observed by Bhushan[1] in earlier studies, and it could be due to nonrecoverable plastic or "viscoplastic" characteristics of the material. Note that PI follows a similar trend to that which was observed for PET.

To enable the acquisition of more creep recovery data, the experiments shown in Figure 7 for PEN, ARAMID, and PBO were only performed for 50 h. The recovery data for these materials are more representative of viscoelastic solids because the majority of the viscoelastic deformation is recovered.

Recovery characteristics for PET, PEN, AR-

AMID, PI, and PBO are shown on an expanded scale in Figure 8. Data sets in this figure were obtained by fitting the data to a general exponential function of the form $e^{-t/\tau}$, where τ is the time constant in hours. This time constant can be thought of as a "recovery time." As a result, the longer the time constant, the longer it takes the material to recover from its viscoelastic deformation. Multiple recovery times could be obtained in a manner similar to that shown in eq. (5) for retardation times associated with creep compliance. However, the use of one exponential term of the form $e^{-t/\tau}$ is sufficient for fitting the recovery data over a relatively short 10–15 h time period. It is important to note that this time constant does not consider the initial creep recovery due to elastic and short-term viscoelastic effects. This is indicated in Figure 7 by the creep compliance value for each of the materials at the end of the experiment. Because PET, PEN, and PI crept more than PBO or ARAMID, they have compliance values at the end of the experiments that are higher than those observed for the other two materials. In other words, they have more viscoelastic deformation to recover. Based on the time constants shown in Figure 8, PEN actually recovers more quickly than the other materials. The time constant for PEN is 7.3 h, which means that it takes approximately 7 h for PEN to recover 1/e or 37% of its viscoelastic deformation. In comparison, PET takes 14 h and ARAMID takes approximately 12 h to recover 37% of their viscoelastic deformation. PI and PBO take substantially longer periods of time to recover (42 and 32 h), but PBO has less total deformation to recover than any of the other materials.

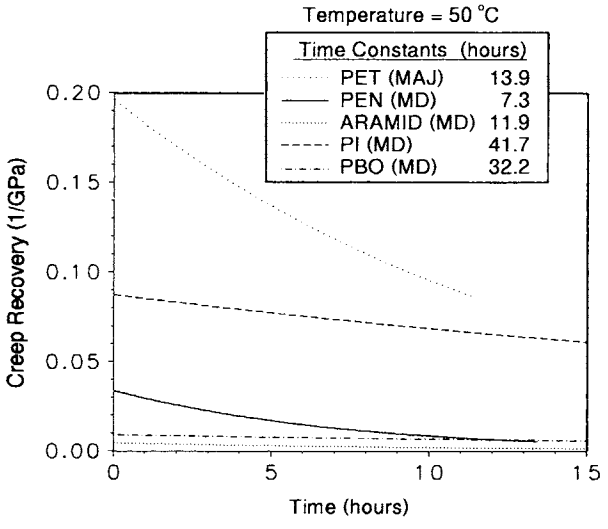

Figure 8 Creep recovery characteristics and time constants for ultrathin polymeric films.

With the exception of PI, the relative magnitudes of the calculated recovery times shown in Figure 8 are comparable to the τ_2 values listed in Table III, because these retardation times are indicative of a 1–10-h time period as are the recovery times in Figure 8. The magnitude of the recovery time for PI is comparable to τ_3 due to the fact that the τ_2 value for this material is on the order of 1 h. (The actual retardation and recovery times cannot be compared exactly because three retardation times were determined for a 100 h creep compliance experiment, and only one recovery time was determined for a 10–15 h creep recovery experiment.) Note that PEN has the lowest τ_2 value as well as the lowest recovery time. ARAMID has the next lowest τ_2 and recovery times followed by PET and PBO. PI has the longest recovery time, which is actually comparable to its τ_3 value.

Prediction of Long-Term Creep Behavior using Time–Temperature Superposition

In addition to the creep experiments at 50°C, experiments were also performed at 25 and 40°C. PET, PEN, ARAMID, PI, and PBO were all evaluated at these different temperature levels in both the machine and transverse directions (major and minor axis for PET). The Marquardt algorithm was also used to curve fit these data sets, and results are shown in Figure 9.

As expected, Figure 9 shows that creep tends to increase with an increase in temperature for all the materials. Furthermore, the data obtained for PET compare well with those obtained by Bhushan.[1] For the polyester materials (PET and PEN) the minor or transverse directions tend to show a total creep compliance which is greater than that measured for the major or machine directions. However, at a given temperature, the rates of creep appear to be similar for these materials regardless of material orientation. PEN shows some fluctuations in creep and creep rate at 40°C, and the cause of these fluctuations is unknown. PET (MIN) shows a rate of creep that increases throughout the experiment, as demonstrated by a slightly concave curve and increasing slope at 40 and 50°C. The liquid crystal polymers (ARAMID and PBO) as well as PI have creep curves in the transverse direction that tend to be lower than those measured in the machine direction. For ARAMID, there appears to be a greater effect of temperature on creep in the transverse direction than in the machine direction, whereas the other materials show similar effects of temperature on creep in both orientations.

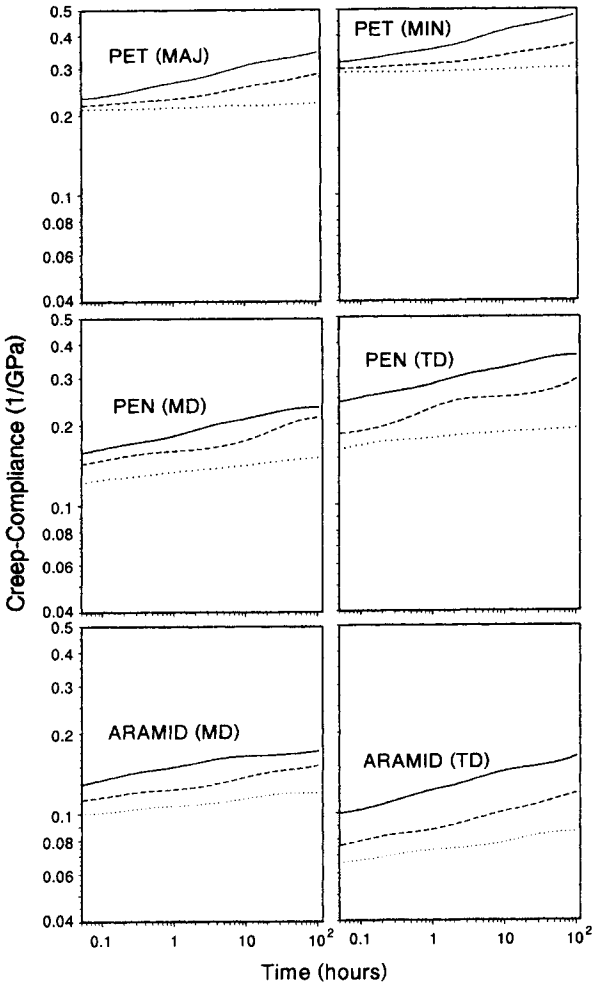

Figure 9 Creep compliance measurements for ultrathin polymeric films at 25, 40, and 50°C.

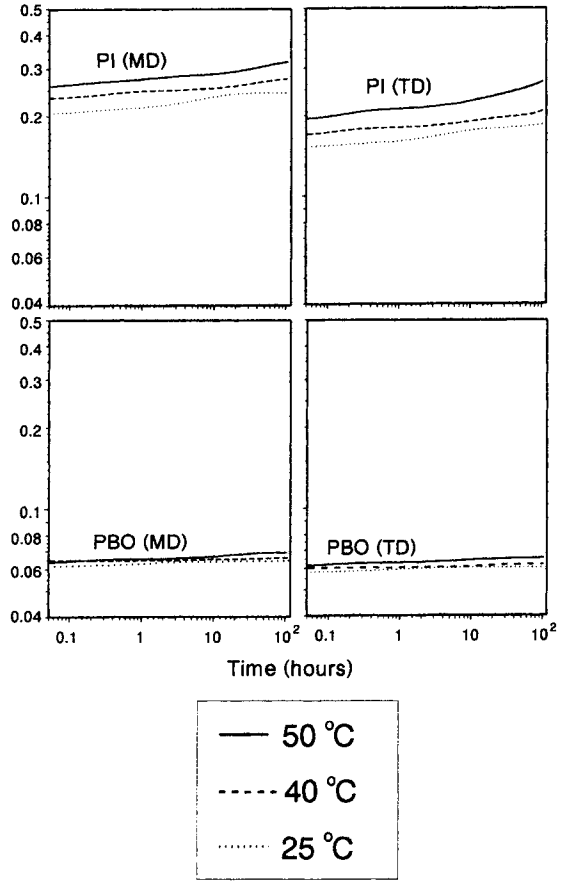

Figure 9 (*Continued*)

An analytical technique known as time–temperature superposition (TTS) has been used to predict long-term creep behavior at ambient temperature.[2,13] For this analysis, creep measurements at the elevated temperature levels shown in Figure 9 are superimposed on one another to predict behavior at longer time periods. The rationale behind this methodology stems from the observation that most polymers will behave in the same compliant manner at a particular high temperature as they will when they are deformed at a particular slow rate at room temperature. In other words, there is a correspondence between time (or rate of deformation) and temperature.

Results from the TTS analysis are presented in Figure 10(a) and (b) for the machine and transverse orientations (major and minor axes for PET). The trend lines (or master curves) for the substrates are assembled to predict the creep compliance at 25°C over a 10^6 h time period. Shift factors tabulated above the figures show how much each curve was shifted (in hours) to enable a smooth fit to be obtained. Creep experiments at temperatures higher than the 25°C reference temperature correspond with longer time periods. Therefore, the 40 and 50°C curves are shifted to the right during the time-temperature superposition analysis. (Note that shifting to the right corresponds with larger *negative* shift factors.)[4] Some vertical shifting is also necessary to accommodate differences in initial elastic response when the materials are loaded as well as differences in elastic moduli at elevated temperatures. However, this vertical shifting rarely exceeds 5% of the total creep compliance measured for a polymer.

At the 25°C reference temperature used to construct Figure 10(a) and (b), PET shows the largest amount of creep along its minor optical axis. PEN and PI show somewhat less creep, whereas ARAMID and PBO have total creep compliances that are significantly lower. These observations were also made using just the 50°C temperature data shown in Figure 5.

Shift Factors, $\log(a_T, h)$ (Reference Temperature = 25 °C)

T (°C)	PET (MAJ)	PEN (MD)	ARAMID (MD)	PI (MD)	PBO (MD)
25	0	0	0	0	0
40	-2.68	-2.93	-2.20	-2.30	-1.68
50	-4.05	-3.74	-4.04	-4.88	-4.14

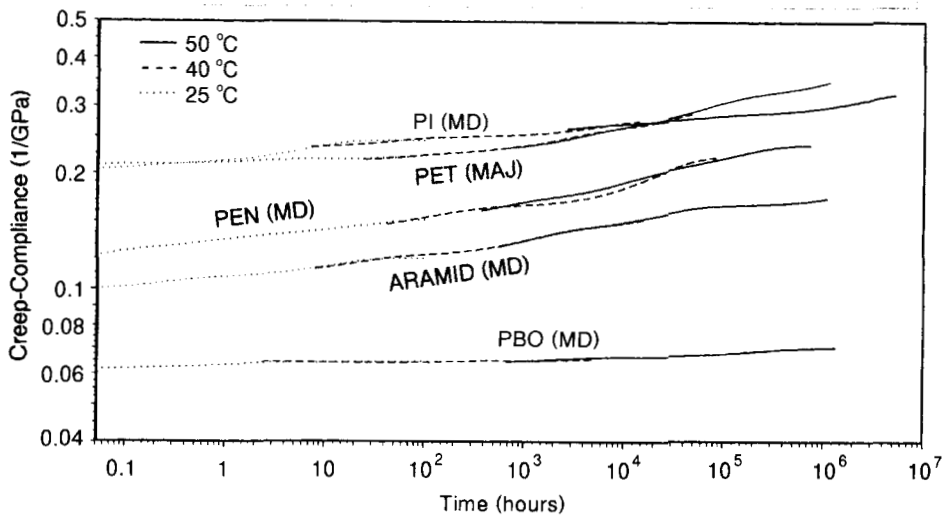

Shift Factors, $\log(a_T, h)$ (Reference Temperature = 25 °C)

T (°C)	PET (MIN)	PEN (TD)	ARAMID (TD)	PI (TD)	PBO (TD)
25	0	0	0	0	0
40	-2.68	-2.75	-2.05	-2.03	-1.83
50	-4.36	-4.55	-4.23	-4.51	-4.10

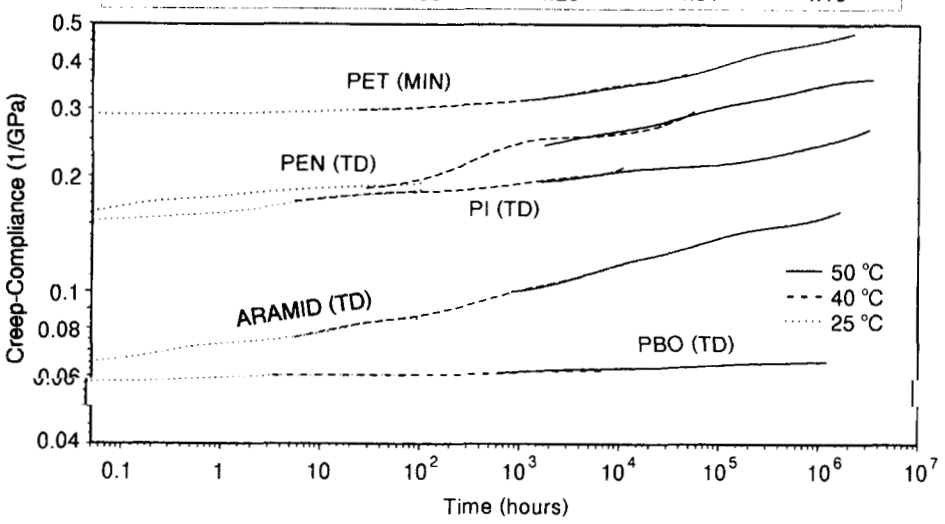

Figure 10 (a) Creep compliance master curves for ultrathin polymeric films. Machine Direction data (Major Optical Axis for PET). (b) Creep compliance master curves for ultrathin polymeric films. Transverse Direction data (Minor Optical Axis for PET).

The rate of creep (or creep velocity) is indicated by the slopes of the curves in Figure 10(a) and (b). Each curve shows relatively small changes in slope throughout the experiments, and results presented in Figure 6 showed the ramifications of these changes using the last decade of the creep data obtained at 50°C. However, it is also useful to consider the overall slope of the master curves from 0.05 to 10^6 h. By examining the data in this manner, it can be seen that PBO has the lowest rate of creep, because the slope of its master curve is relatively low. PI also has a relatively low slope that increases only slightly at longer times. PET has a creep velocity that increases throughout the experiment because the slope of the master curves for both the major and minor axes increase throughout the experiment.

PEN (MD) and ARAMID (MD) have similar rates of creep that are actually higher than the rate of creep for PET (MD) at shorter times. ARAMID (TD) has a higher creep velocity than all the other materials with a slope that is relatively steep and constant. Due to the lack of a smooth master curve for PEN (MD & TD) it is questionable whether the time–temperature superposition technique is applicable for this material. However, the master curve is still included to assist with the prediction of PEN's creep behavior at longer time periods when it is used as a substrate for magnetic tapes.

From the time–temperature superposition analysis shift factors are obtained for each temperature. These shift factors can be used to predict the activation energy for the creep compliance process. An Arrhenius relationship shown below is used to make this prediction for so-called secondary relaxations (or motions) in the material.[1,4,14]

$$\log a_T = \frac{-\Delta H}{R(2.303)}\left[\frac{1}{T_r} - \frac{1}{T}\right] \tag{6}$$

where,

$\log a_T \equiv$ shift factors from time–temperature superposition analysis.
$\Delta H \equiv$ activation energy in kJ/mol.
$R \equiv$ *gas constant = 8.3145 J/(mol°K).*
$T_r \equiv$ reference temperature from TTS master curve (in °K).
$T \equiv$ experimental temperature corresponding to shift factor (in °K).

Equation (6) is derived from the following assumed relationship for retardation times (Eq. 7), and the mathematical expression for time–temperature superposition shown in Eqs. 8(a) and (b).

$$\tau_k(T) = A_k \exp(\Delta H/RT) \tag{7}$$

$$D(t, T) = D(t/a_T, T_r) \tag{8a}$$

$$\sum_{k=1}^{K} D_k(T)\,[1 - e^{-t/\tau_k(T)}] = \sum_{k=1}^{K} D_k(T_r)\,[1 - e^{-t/a_T\tau_k(T_r)}] \tag{8b}$$

where,

$\tau_k(T), \tau_k(T_r) \equiv$ discrete retardation times at temperature T, and reference temperature T_r.
$D_k(T), D_k(T_r) \equiv$ discrete compliance terms at temperature T, and reference temperature T_r.
$t/a_T \equiv$ reduced time from time–temperature superposition master curves.
$A_k \equiv$ a constant.

Equations (7) and (8) can be interpreted as follows: higher activation energies at a given temperature lead to higher retardation times, which in turn, influence the magnitude of the delayed compliance $D_k(T)[1 - \exp(-t/\tau_k(T))]$.[3] Note that the $D_k(T)$ terms in Eq. 8(b) are assumed to be independent of temperature for the derivation of Eq. (6). Furthermore, the activation energy ΔH should be interpreted as the energy required to activate the molecular process that causes creep.

Using Eq. (6), ΔH can be determined by plotting $\log a_T$ against $1/T$ and using linear regression to determine the slope of the best-fit line. Figure 11 shows the results of this regression analysis. Note that the data points for the two polyesters (PET and PEN) fall on the same line, and the slopes are nearly identical at 311 and 309 kJ/mol. However, the maximum confidence intervals for these regression lines are ±5 and ±11 kJ/mol for PET and PEN, respectively. Therefore, there is no statistical difference between these ΔH values. Previous research by Bhushan[1] has shown that the activation energy for PET creep is around 200–240 kJ/mol. The higher activation energy for the current PET sample could be due to improvements in processing of PET. ARAMID and PBO have similar slopes of 300 and 295 kJ/mol. However, the confidence intervals overlap yielding little significance to differences in activation energy.

A linear Arrhenius plot suggests that the molecular motions are secondary or short range in nature.[4] From Figure 11 this is certainly true for PET and PEN, and reasonably true for ARAMID, PI, and PBO, although the scatter for these materials is somewhat larger. A nonlinear $\log a_T$ vs. $1/T$ plot is usually fitted to the WLF equation,[13] but this equation is typically valid for viscoelastic data acquired at a wider range of temperatures through the glass transition temperature, T_g. Because the experiments presented herein were performed below T_g, the use of Eq. (6) as well as the linearity of the $\log a_T$ vs. $1/T$ curve are valid. The only exception to this may be the PET experiments. Although they were performed below T_g and Figure 11 shows a linear shift factor curve, the 100 h duration of the 50°C experiments could have provided enough time for some reorientation of the macromolecules in the amorphous region. Such reorientation of the macromolecules occurs at the T_g and requires an activation energy of 363 kJ/mol for semicrystalline PET.[14] Because the measured activation energy for PET is

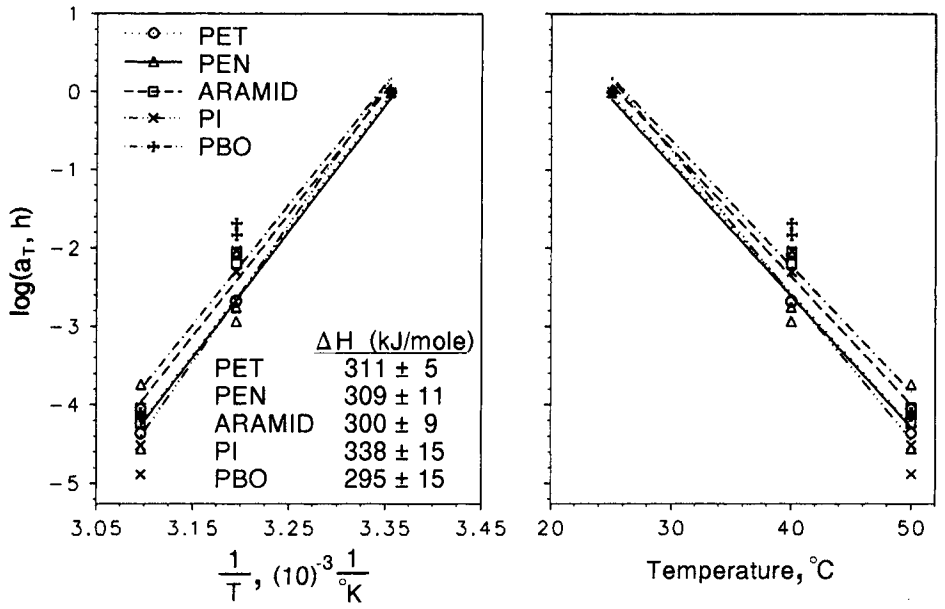

Figure 11 Temperature dependence of shift factors, log a_T, obtained from time–temperature superposition.

311 ± 5 kJ/mol, the large-scale reorientation of molecules in PET is unlikely to have taken place, and the nature of the creep process for PET is short range or secondary motion of the molecules. The nature of the creep process for the other materials would also be secondary motion due to the higher glass transition temperatures and melting points for these materials.

Relationship between Polymeric Structure and Creep Behavior

From the preceding analysis, creep behavior for the polymeric films can be related to short-range or secondary motions. These secondary motions involve the motion of main chain groups and/or side groups, and distortion of the macromolecules will occur through intermolecular distances.[4] These distances are determined by the type of intermolecular bonding between macromolecules.

For the semicrystalline polyester materials (PET and PEN) the location of these intermolecular forces needs to be determined. Ward[15] has stated that there is no clear distinction between secondary relaxations (or motions) in amorphous and crystalline regions. However, results presented herein suggest that the intermolecular distortions that determine creep response for the polyesters are prevalent in the crystalline region. There are clear differences in creep response along the major and minor optical axes for PET, and in the machine and transverse directions for PEN. Because these directions are directly related to crystalline orientation, then the creep must be related to distortions in these regions of the polymers. McCrum et al.[14] have noted that the response of polyesters can be attributed to motions of the COO groups. Thus, creep behavior for PET and PEN could be due in part to rearrangement of these groups in the main chain of the polymers. However, orientation of the macromolecules and intermolecular forces obviously play a role.[4] Although actual slippage of the chains is unlikely below T_g, distortion of the intermolecular bonds between chains such as van der Waals attractions contribute to the creep process. This is demonstrated by higher creep along the minor axis of PET. The stress is applied transverse to the covalently bonded backbone of the molecule, and the material creeps substantially due to distortion through intermolecular distances. The material is not permanently deformed because of the presence of molecules in the amorphous region that happen to be oriented in the direction of the applied stress. Along the major optical axis intermolecular bonds are not as easily distorted, the covalently bonded backbone rigidly resists the applied stress, and creep is lower.

The same arguments can be made for the more advanced polyester film PEN. Creep is higher in the transverse direction than in the machine direction due to the relatively weak intermolecular forces between chains in the crystalline region. Creep results for PEN are typically less than those for PET due

to the presence of the naphthalene group vs. the benzene group for PET. This group not only increases the rigidity of the backbone, but inhibits crystallization due to its more complex stereochemical structure. As a result, more molecules are left frozen in an amorphous state at random orientations to respond to applied stresses from any direction.

Secondary creep and relaxation phenomena in aliphatic polyamide materials have been attributed to motion of $-NH_2$ and $-OH$ chain end groups as well as motion of chain segments that are not intermolecularly bonded to neighboring chains.[14] Because the ARAMID material evaluated herein is an aromatic polyamide, similar mechanisms should contribute to its creep behavior. From Figure 2 and the discussion on test specimens, aromatic polyamides tend to be highly oriented materials with rigid rod-like structures that are formed from liquid crystal solutions.[9] Hydrogen bonds between chains are the only "weak link" in the structure, but the hydrogen bonding in polyamide materials is inherently stronger than the intermolecular bonds in the polyester films. As a result, the total creep compliance tends to be lower for the ARAMID material. The higher creep for the machine direction vs. the transverse direction could be due to the motion and interaction of the $-NH_2$ and $-OH$ end groups in ARAMID. Single intermolecular bonds between the ends of the polymeric chain could be distorted more than the multiple hydrogen bonds between the sides of the chains. Furthermore, depending on how the film is cast, the liquid crystals could also have preferential orientation in one direction vs. another, and intermolecular bonds between crystals could distort leading to creep.

Because measurements for PI are similar to those measured for PET and PEN, it is reasonable to assume that the creep mechanisms are similar. However, from the master curves shown in Figure 10(a), PI (MD) has a more constant rate of creep than PET or PEN until the final decades. This flatter creep response for PI (MD) could be due to the fact that the COO group that contributes to the creep of PET is not entirely present in PI (MD). Only the $C{=}O$ group is present, which cannot move into as many conformational states as the COO group in PET. Due to the presence of multiple aromatic rings, PI would also be expected to have a more three-dimensional structure than PET, which could prevent distortion and slippage of the chains. This could explain the lower total creep for PI in the transverse direction.

PBO is another liquid crystalline polymer with melt characteristics similar to that of ARAMID. Its rigid rod-like structure leads to the lowest creep compliance of any of the materials. Creep is virtually immeasurable, and as indicated for ARAMID, only intermolecular attractions between the crystals are likely to contribute to creep.

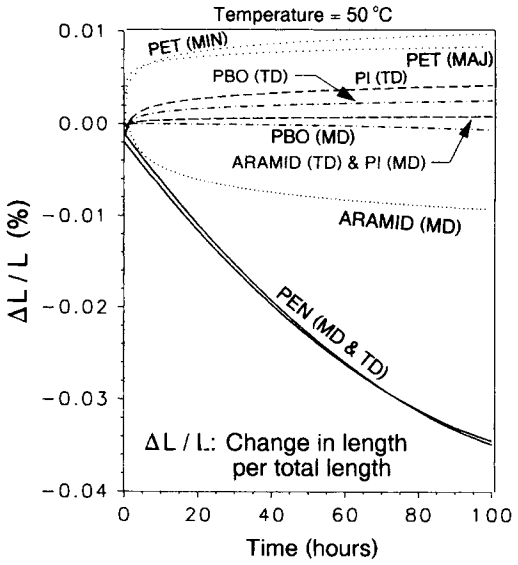

Figure 12 Shrinkage measurements for ultrathin polymeric films.

Shrinkage

Shrinkage results are shown in Figure 12 for the 50°C temperature level. Only ARAMID (MD) and PEN (MD and TD) shrink at this temperature. PEN shrinks as much as 0.035% after 100 h, and ARAMID (MD) shrinks 0.01% after 100 h. For PET, creep appears to be a more dominant factor because its change in length is positive rather than negative. No appreciable amount of shrinkage was measured for PI, PBO, and ARAMID (TD).

The shrinkage behavior shown in Fig. 12 can be directly related to the polymeric structure of the films. Shrinkage is a nonrecoverable deformation process which can be attributed to relaxation of partially-oriented molecules in the amorphous regions of the polymer.[1] (Visualize the partially-oriented molecules as being extended in the amorphous phase. When the temperature is increased, these molecules contract or recoil.) Note that the partially-oriented molecules in the amorphous region should not be confused with the highly ordered (and highly oriented) molecules present in the crystalline regions of the polymer. The crystalline regions in fact do not contribute to shrinkage behavior. Lastly, the relaxation of the partially-oriented molecules in the

amorphous region could result in removal of the residual stresses formed during the processing of the film. As a result, an overall contraction of the film occurs in the direction of the partially-oriented molecules.

PET has been observed to undergo a great deal of shrinkage at temperatures above its glass transition temperature, which is typically 70–120°C.[1,6,16] Below its glass transition temperature the partially oriented molecules in PET can be considered to be "frozen" into immovable conformations. Because the results shown in Figure 12 were for a 50°C temperature level, this could provide an explanation for the lack of PET shrinkage. However, PEN has a glass transition temperature that has been measured to be 156°C,[12] yet it shrinks considerably at 50°C. A conclusive explanation cannot be provided for this behavior, but the naphthalene ring in PEN could sterically inhibit crystallization during processing of this polymer. This so-called steric hinderance could prevent the formation of highly ordered crystalline regions. Instead, during the film manufacturing process, some of the PEN macromolecules are frozen into a partially oriented amorphous phase upon cooling. When the polymer is heated, energy is imparted to the partially-oriented molecules to allow them to reorient themselves to shorter lengths.

ARAMID (TD) and PBO show no appreciable shrinkage because they have rigid rod-like structures that exhibit a high degree of orientation. They are often referred to as liquid crystal polymers because they form oriented liquid crystalline arrays in solution.[6,9] This characteristic is what enables the formation of high strength, high modulus ARAMID and PBO films. However, some shrinkage is observed for ARAMID (MD). This behavior could be indicative of the atypical sulfone groups present in the backbone of the ARAMID material Mictron™ evaluated in this research (see Fig. 2). Fibrous ARAMID materials such as Kevlar™ do not have this sulfone group, which may inhibit crystallization and lead to shrinkage from the rearrangement of partially oriented molecules.

As a final note, polyimide (PI) does not show any measurable shrinkage. Although polyimides are known to have a relatively low crystallinity (15–20% for PI vs. 50–60% for PET), typical polyimides have an extremely high glass transition temperature of 360–410°C.[1] Therefore, substantial shrinkage would not be expected for PI below its glass transition.

When comparing shrinkage measurements presented herein with those reported by others, it is important to note that *all* the shrinkage measurements presented in this article were performed at 50°C, which is the upper use limit for magnetic tape substrates. Perettie and Pierini[6] have presented shrinkage measurements taken over a 5-min interval at 200°C for PET, PEN, ARAMID, PBO, and a polyimide (Kapton™), which is similar to Upilex™. Because PET and PEN are above their T_gs at 200°C, they shrink 5–10% and 1.5%, respectively. ARAMID and the polyimide shrink 0.1% at 200°C, and PBO shrinks less than 0.1% at this temperature.[6] Ashton[16] has reported shrinkage values of 1.0% for PET at 100°C over a 30-min time period. Note that these shrinkage values are two to three orders of magnitude higher than what was reported herein due to the higher temperatures used by the other researchers.[6,16] Note that when PET is tested above its T_g, it will shrink more than PEN.[6] However, at the 50°C temperature level used in the present research, PEN shrinks more than PET possibly due to residual stresses resulting from the manufacturing process, and the shrinkage measured for PEN could be alleviated by stress-stabilizing the material at 65°C.[1,17]

SUMMARY AND CONCLUSIONS

Viscoelastic and shrinkage characteristics of five ultrathin polymeric films have been evaluated. These films include PET, which is currently the standard polymeric film used for magnetic tape substrates; PEN and ARAMID, which are beginning to see some use as substrates; and PI and PBO, which are developmental materials being considered for this application. A creep tester was used to measure creep and shrinkage properties of the films. Creep compliance data sets were fitted to the Kelvin–Voigt model using the Levenberg–Marquardt algorithm, and three-spring dashpot elements were typically required to fit the data.

Creep compliance measurements at 50°C show that PEN, ARAMID, PI, and PBO offer improvements in viscoelastic behavior when compared to PET. PEN and PI have total creep compliances, which are 0.05 to 0.25 GPa^{-1} less than those measured for PET depending on the orientation. In comparison, the total creep compliance for ARAMID is 0.20 to 0.30 GPa^{-1} lower than PET's, and PBO has a creep compliance that is as much as 0.40 GPa^{-1} less than that measured for PET. These results also indicate that the viscoelastic behavior of the polyester materials (PET and PEN) is more anisotropic when compared to ARAMID, PI, and PBO. Creep velocity measurements indicate that PET and PI have high rates of creep, PBO creeps at a comparatively low rate, PEN has a creep velocity after 100 h which has a decreasing trend, and AR-

AMID creeps at a constant rate. Recovery characteristics were also measured and are similar to the creep characteristics with the exception of PET and PI, which do not completely recover all of their creep deformation.

Creep data acquired at 25, 40, and 50°C were used to predict long-term creep at ambient temperature. Results from this time–temperature superposition technique showed that the total creep compliance for PET is typically higher at longer time periods (10^6–10^7 h) than that measured for the other materials. However, the time–temperature superposition technique showed that the ARAMID material has a higher creep velocity with a slope that is relatively steep and constant. Recall that a similar observation was made using the creep velocity data at 50°C.

Shift factors obtained from time–temperature superposition were used to predict activation energies for the creep compliance processes. ΔH values from the linear slopes of Arrhenius plots were found to be similar for all the materials, and approximately equal to 300 kJ/mol. Because this activation energy is below that required for large scale molecular motion indicative of the glass transition temperature, the creep process must involve molecular motions that are secondary or short range in nature.

Creep behavior for the polyesters seemed to be dictated by intermolecular distortions and secondary motions of COO groups in the crystalline domains of these materials. Differences in creep behavior for PET vs. PEN can be attributed to the naphthalene group in PEN, which not only increases the rigidity of the macromolecular backbone, but inhibits crystallization leaving unoriented and partially oriented molecules in the amorphous state. Although these molecules in the amorphous state can inhibit creep, they can also lead to residual stresses and shrinkage of PEN. This is indeed the case because shrinkage was measured to be 0.035% for PEN after 100 h at 50°C. Postannealing of polyester films to relieve these residual stresses is a well-documented process that has been studied extensively for PET.[1]

ARAMID and PBO tend to show lower creep and shrinkage behavior due to their rigid rod-like structures indicative of liquid crystal polymers. Although PBO shows minimal creep and low shrinkage, ARAMID tends to have a constant creep velocity, and shows some shrinkage along the machine direction. This behavior could be related to the presence of the sulfone group in the ARAMID material (see Fig. 2). Other fibrous aromatic polyamides such as Kevlar™ do not contain the sulfone group, and are therefore strongly hydrogen bonded. The presence of the sulfone group will prevent such bonds from continuously forming between chains in the ARAMID material.

For reasons already discussed, after 100 h at 50°C PEN and ARAMID (MD) shrink 0.035% and 0.01%, respectively. However, shrinkage results show that the other polymeric films do not shrink at 50°C. Because appreciable shrinkage typically only occurs above the glass transition temperature, negligible shrinkage at 50°C is an expected result for the polymers studied in this research.

Because the polymeric films evaluated in this research are potential alternative substrate materials for magnetic tapes, it is appropriate to discuss their characteristics in light of this application. In general, the alternative substrates offer improvements in viscoelastic and shrinkage characteristics when compared to PET. PBO offers the greatest improvements but is currently unavailable. PI offers only slight improvements in creep properties, and its availability is also in question. PEN and ARAMID creep less than PET, and they both have lower creep velocities than PET, which renders them less susceptible to stretching, damage, and long-term reliability problems discussed in the Introduction. In addition, the creep velocity for PEN continues to decrease after 100 h at 50°C, which possibly makes it a more suitable substrate material because ARAMID tends to deform at a constant rate. Therefore, even though the particular PEN and ARAMID (MD) materials evaluated in this research shrink more than PET at 50°C, both of these materials have creep characteristics which make them suitable replacements for PET, and the shrinkage problems could be alleviated through better processing controls.[1,12,17] It is also important to note that PET and PEN are drawn films, and are therefore less expensive than ARAMID, PI, and PBO, which are cast films. In conclusion, the choices for alternative magnetic tape substrates can be ranked as follows: 1st choice—PBO (unavailable), 2nd choice—PEN or ARAMID, 3rd choice—PI (availability in question), 4th choice—PET.

This project was sponsored by the National Storage Industry Consortium/Advanced Research Projects Agency (Grant MDA 972-93-1-0009). We would like to thank Mr. W. Wilson of Dupont Imaging Systems/Medical Products, Florence, SC, for supplying 57 DB Mylar™ (PET) films, Mr. K. Irobe of Teijin–Dupont Films, Atlanta, GA, for Teonex™ (tensilized PEN) films (used in the 3M QIC data cartridge DC 2120XL), Mr. T. Kondo of Toray Industries, Inc., New York, for Mictron™ TX-1 (ARAMID) films (used in the Sony NTC-90 Digital Micro Tapes),

Ube, Japan, for Upilex™ (polyimide) films, and Dr. D. J. Perettie of The Dow Chemical Co., Midland, MI, for hand-drawn/unbalanced/isotropic experimental PBO films. Technical discussions with Dr. Jim Eaton of NSIC are gratefully acknowledged.

REFERENCES

1. B. Bhushan, *Mechanics and Reliability of Flexible Magnetic Media,* Springer-Verlag, New York, 1992.
2. J. D. Ferry, *Viscoelastic Properties of Polymers,* 3rd ed., Wiley, New York, 1980.
3. N. W. Tschoegl, *The Phenomenological Theory of Linear Viscoelastic Behavior: An Introduction,* Springer-Verlag, New York, 1989.
4. J. J. Aklonis and W. J. MacKnight, *Introduction to Polymer Viscoelasticity,* Wiley, New York, 1983.
5. B. Bhushan and D. Connolly, *ASLE Trans.,* **29,** 489–499 (1986).
6. D. Perettie and P. Pierini, in *Advances in Magnetic Recording,* D. Speliotis, Ed., Elsevier, Amsterdam, to appear.
7. D. Perettie, W. Hwang, P. Pierini, D. Speliotis, J. Judy, and Q. Chen, *J. Mag. Magn. Mater.,* **120,** 334–337 (1993).
8. D. Perettie and D. Speliotis, *J. Mag. Soc. Jpn.,* **18**(S1), 279–282 (1994).
9. A. Rudin, *The Elements of Polymer Science and Engineering: An Introductory Text for Engineers and Chemists,* Academic Press, New York, 1982.
10. C. Bourgerette, A. Oberlin, and M. Inagaki, *J. Mater., Res.,* **8,** 121–122 (1993).
11. W. H. Press, B. P. Flannery, S. A. Teukolsky, and W. T. Vetterling, *Numerical Recipes in C: the Art of Scientific Computing,* Cambridge University Press, New York, 1988.
12. B. L. Weick and B. Bhushan, *IEEE Trans. Mag.,* to appear.
13. M. L. Williams, R. F. Landel, and J. D. Ferry, *J. Am. Chem. Soc.,* **77,** 3701–3707 (1955).
14. N. G. McCrum, B. E. Read, and G. Williams, *Anelastic and Dielectric Effects in Polymeric Solids,* John Wiley, New York, 1967.
15. I. M. Ward, *Mechanical Properties of Solid Polymers,* Wiley-Interscience, New York, 1971.
16. G. Ashton, *PET Substrate Properties in Flexible Magnetic Media,* National Media Lab Tech. Report RE-0009, St. Paul, MN, May 1993.
17. K. Irobe, Teijin Dupont Films, Atlanta, GA (personal communication).

Received February 28, 1995
Accepted June 6, 1995